Model Predictions and Observed Performance of JWST's Cryogenic Position Metrology System

Sharon R. Lunt[a], David Rhodes[a], Andrew DiAntonio[a], John Boland[a], Conrad Wells[a], Trevis Gigliotti[b], Gary Johanning[c]
[a]Harris Corp, 400 Initiative Drive, P.O. Box 60488, Rochester, NY, USA 14606-0488; [b] Principal Point Geospatial Solutions, Hamilton, Ontario, Canada; [c]Geodetic Systems, Inc., 1511 Riverview Dr, Melbourne, FL 32901

ABSTRACT

The James Webb Space Telescope cryogenic testing requires measurement systems that both obtain a very high degree of accuracy and can function in that environment. Close-range photogrammetry was identified as meeting those criteria.

Testing the capability of a close-range photogrammetric system prior to its existence is a challenging problem. Computer simulation was chosen over building a scaled mock-up to allow for increased flexibility in testing various configurations.

Extensive validation work was done to ensure that the actual as-built system meet accuracy and repeatability requirements. The simulated image data predicted the uncertainty in measurement to be within specification and this prediction was borne out experimentally. Uncertainty at all levels was verified experimentally to be <0.1 mm.

Keywords: James Webb Space Telescope, JWST, photogrammetry, CPM, cryogenic testing

1. INTRODUCTION

Close range photogrammetry has been successfully used on large hardware systems such as the Microwave Anisotropy Probe (MAP) [1] for dimensional surveys of large numbers of points. Photogrammetry was also the approach selected at Goddard Space Flight Center (GSFC) for the James Webb Space Telescope (JWST) Integrated Science Instrument Module (ISIM) testing at cryogenic temperatures.[2] Typical uncertainty requirements for such work is +/- 100 micron, 2 sigma, per axis, per target point. Due to the rigid requirements photogrammetry was chosen the as a candidate for use as the Cryo-Position Metrology (CPM) system for the Optical Telescope Element and ISIM (OTIS) thermal vacuum (T/V) tests to be performed in Chamber A at Johnson Space Center (JSC).

Prior to the construction and installation of the CPM the expected accuracy of the as designed system needed to be validated. Due to the size and complexity of the OTIS structure, the creation of a computer model was chosen rather than a mock up for greater flexibility in examining various testing configurations and to provide a test bed that can be used for the life of the program. This paper summarizes work that was done to assess the expected accuracy of measurements for the OTIS configuration before any hardware was installed in the chamber and chamber. Predictions are then compared to subsequent verification measurements of the operational CPM performed during initial chamber tests of Ground Support Equipment (GSE) to be used in the full OTIS tests. The predicted and actual performance met the requirements of the error budget and the system has been successfully utilized in several optical tests utilizing the JWST Pathfinder.[3].

2. HARDWARE DESCRIPTION

For T/V tests of the JWST observatory, a set of four cameras on rotating windmill booms and located within the pressure and thermal tight enclosures are used inside the helium shroud. As the windmills rotate, the camera system records multiple images of special photogrammetry targets placed on and about the OTE. Figure 1 provides an overview of the JWST OTIS Flight Hardware and OGSE in the JSC Chamber A. The OTIS photogrammetric survey will be done

primarily during conditions of a 30K vacuum environment, although some testing will be done at ambient temperature and during cool down/warm up.

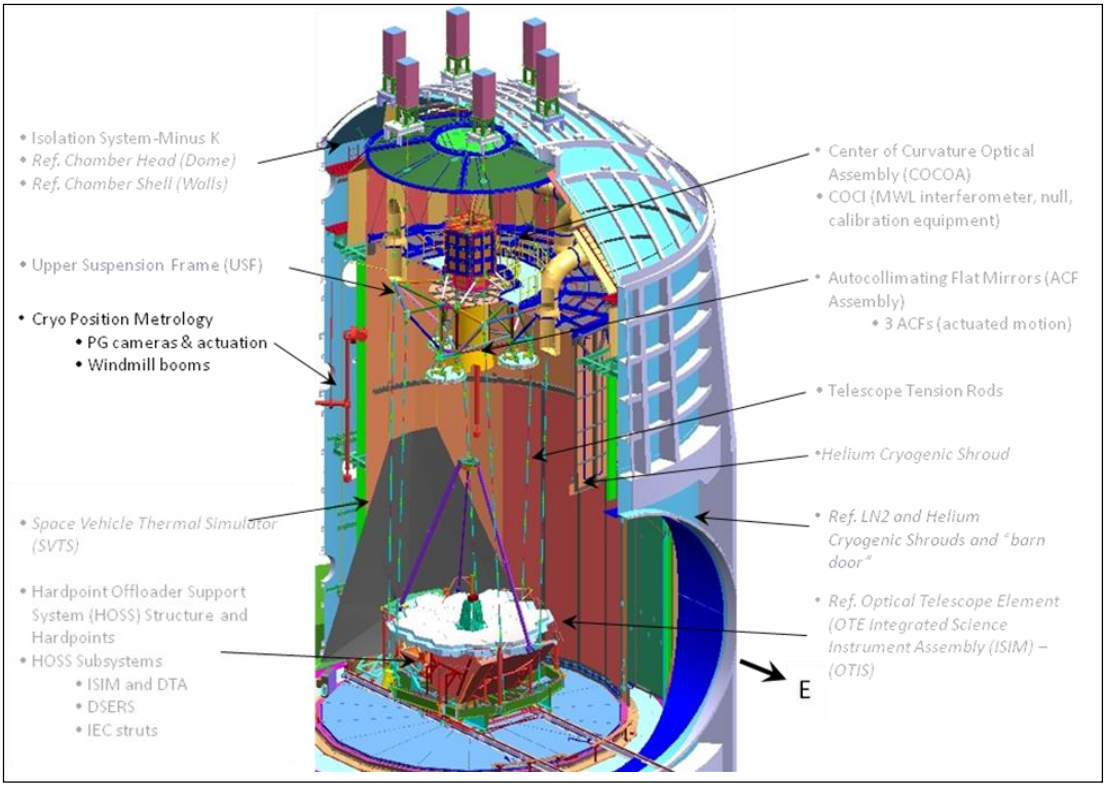

Figure 1 Overview of JWST OTIS Flight Hardware and OGSE in JSC Chamber

The successful application of photogrammetry requires support equipment that includes scale bars, code targets to aid automated processing and metrology target point locations that define the object of interest. The correct calculation of scale to apply to a photogrammetric bundle is of critical importance to the overall accuracy of a measurement survey.

2.1 Scale Bars

To scale a photogrammetric measurement, at least one known distance must be present in the imagery. For the purposes of the JWST PG system multiple scale fixtures (i.e. scale bars) are incorporated into the object space that contain target pairs of known distances. The distances between target pairs on the bar are characterized and known and can be used to scale the measurement survey. Multiple distances allow a higher order of scale calculation accuracy and the ability to find scale errors. Thermal sensors are required on each bar to accurately calculate scale bar length at each point in the temperature cycle where a measurement is performed.

The modeled setup for this PG application includes 20 invar scale bars positioned around the primary mirror from posts attached to the HOSS structure. Figure 2 shows the distribution and an example invar scale bar

Each scale bar contains one thermal diode and a set of four target pairs for redundant scale. In addition as part of the gravity references located on the posts there are 5 vertical scale bars for vertical (Z) scale.

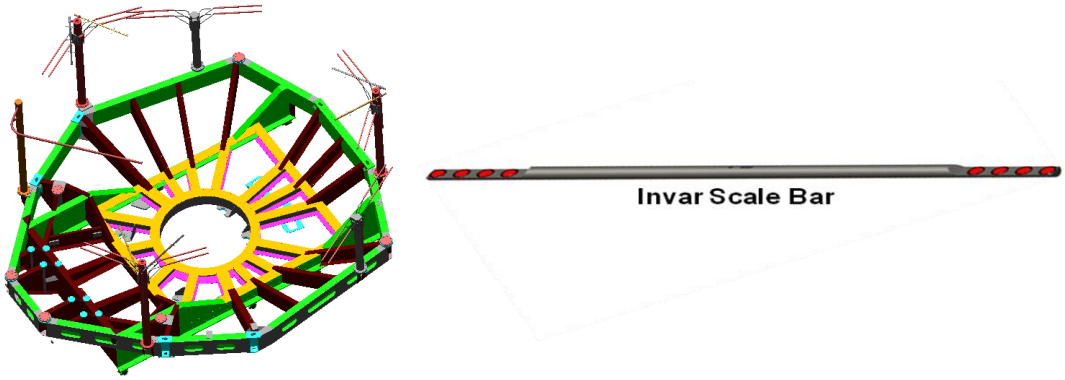

Figure 2 Distribution of invar scale bars around the HOSS and example invar scale bar

2.2 Code Targets

Code targets are a special type of target that the V-STARS software can recognize, automatically decode and use to automatically calculate the position and orientation of the camera to aid bundle adjustment. Each code is made up of a unique pattern of dots. When planning a photogrammetry project code targets must be well distributed throughout the object space so that each captured image contains a minimum of 4 code targets. Code targets were distributed on the chamber wall and on sleeves which went around the telescope road supports. In addition, the telescope rod sleeves provide PG targets in what would otherwise be empty space so that there is sufficient points in each image to stitch the entire bundle together. Initially, the points on the telescope rods were also to be used as scale bars, but measurements of expected Coefficient of Moisture Expance (CME) and Coefficient of Thermal Expansion (CTE)indicated that the materials properties were too variable to ensure reliable scale bar accuracy. An illustration of the telescope rod sleeve is shown in Figure 3.

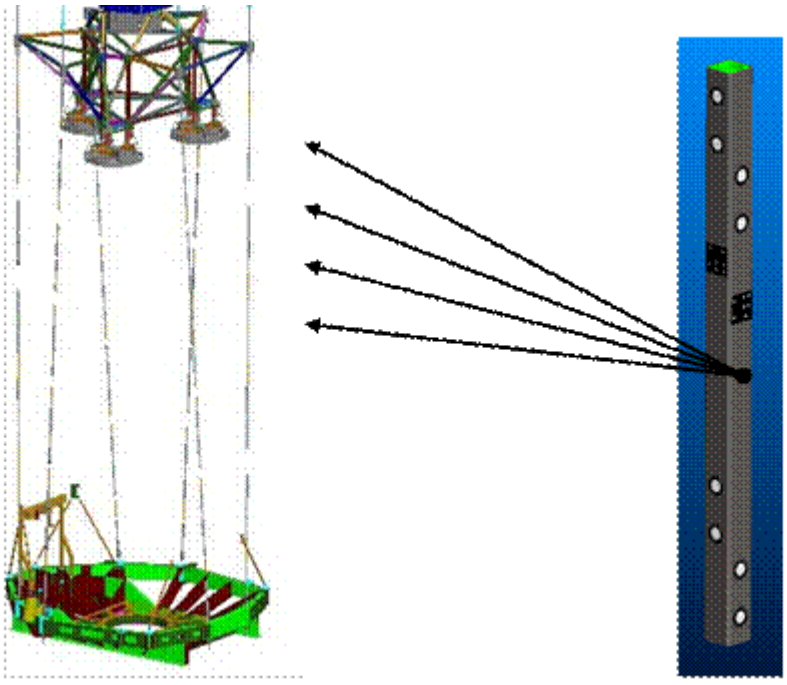

Figure 3 Distribution of composite sleeves on the telescope rods and example composite sleeve

2.3 INCA Camera System

The photogrammetric camera system selected for the JWST photogrammetric application is the third generation INtelligent CAmera (INCA3) system provided by GSI. In addition to its robust design and vetted operational accuracy this system was chosen because it could operate in an automated capacity. Due to the demands of the cryogenic vacuum tests at JSC remote operation was an important capability. A compact but powerful PC accompanies the camera system

and can store images directly to hard disks or connected to a network via a one-cable interface port. Figure 4 shows the INCA3 photogrammetric camera system and identifies some of the advanced features.

Figure 4 INCA3 Camera system as provide by Geodetic Systems Inc.

Table 1outlines the manufacturer's specifications for the INCA3 camera system.

Table 1 Manufacturer's specifications for the INCA3 camera system

Characteristic	Values
Sensor	3500 x 2350, 12-bit, 8MP
Field of View	77º x 56º
Accuracy	5 µm + 5µm/m (0.025mm @ 4m, 0.001" @ 160")
Lens Focal Length	21mm
F Stop	F/16
Pixel Size	10 µm square

3. DATA PROCESSING

All PG data analysis was completed using the Video, Self-Calibration, Triangulation and Resection Software (V-STARS) supplied by GSI to create a bundle adjustment. A bundle adjustment determines the 3D coordinates of the targeted feature points in an automated operation from imagery taken at multiple points of view. The adjustment eliminates systematic error and minimizes residual random error through a least squares process that accounts for the position and orientation of the cameras when each image was captured and distortions from the camera lens. The 3D coordinates created as the output of the bundle adjustment process are then aligned to the desired coordinate system and provide the measured position of all targets.

For most runs, no bad or weak point filtering was applied other than that done automatically by V-STARS as removal of all identified weak points resulted in the elimination of many desired targets, though there was a rejection limit set for minimum number of rays (images) required per point. A check variation was done where bad and weak points were manually removed and the resulting uncertainty estimates of the remaining points were determined to be equivalent. The selection of scale bars was found to be a critical factor in absolute accuracy level, and is discussed in more detail in Section 6.3.

4. MODEL CONSTRUCTION

The computer model was constructed using the **D**igital **I**mage and **R**emote **S**ensing **I**mage **G**eneration (DIRSIG) version 4.5 software developed by Rochester Institute of Technology Digital Image and Remote Sensing Laboratory and has been used extensively throughout the remote sensing community for more than 20 years.[4] DIRSIG performs end-to-end radiometric calculations from source to detector.

In order to determine the distance and angle fall-off of the reflective material, extensive testing of actual targets at various sizes, angles, and distances was done with the INCA3 camera. The model was verified to have the correct number of pixels for a target and intensity profile.

By importing the CAD model of the OTIS configuration as well as the material properties of 3M retro reflective material used for the photogrammetry target material (illumination response, fall-off due to look angle), a realistic model of the structures such as the PM, SM, etc. were constructed to identify hardware occlusions and refine target locations in the configuration shown in Figure 1. The camera positioning and movement was incorporated into the definition of each modeled image. In addition, image processing after the computer model generation was used to simulate sensor response and an adequate point spread function of the INCA camera system, and then converted to 8-bit to match the INCA 3 camera system. The images were then imported into V-STARS for processing to determine the predicted PG measures of each point. An example of a DIRSIG generated and post processed image is shown in Figure 5 below.

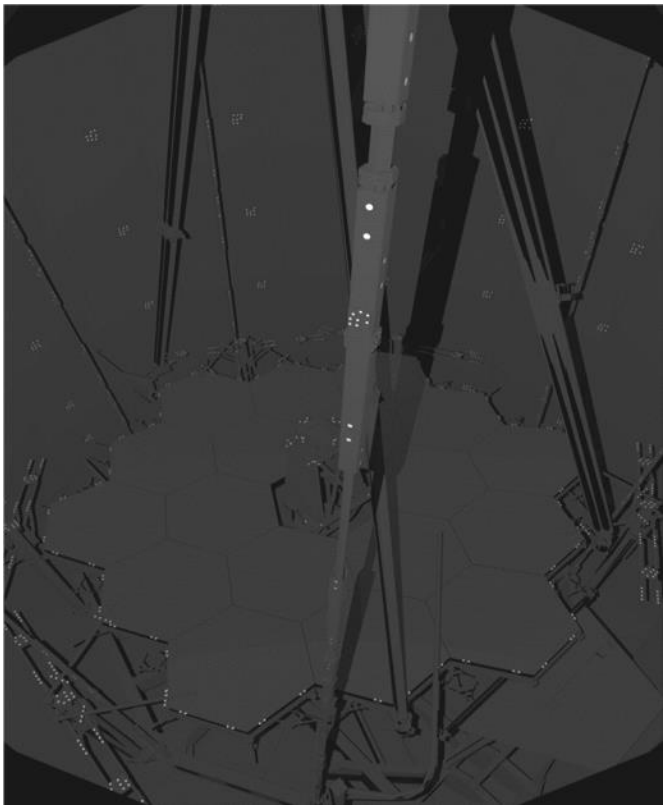

Figure 5. Sample DIRSIG image

5. HARDWARE TESTING CONFIGURATIONS

The performance of the CPM was evaluated during the initial Chamber Commissioning Testing (CCT) T/V tests and follow-onwork was performed during Optical Ground Support Equipment (OGSE) 1 & 2 chamber T/V tests.

5.1 Chamber Commissioning Testing

The hardware configuration used for the PG commissioning had calibration fixtures at various heights appropriate to the key components of OTIS and spread across the PM footprint. There are a total of 8 calibration plates arranged as described below. A diagram of the target arrangement is shown in Figure 6.

- 1 at the ACF level attached to the ACF load simulator
- 1 at the SM level attached to a telescope rod support
- 1 at the AOS level on a 80/20 mount attached to the load sled
- 4 on the load sled with 2 positioned on the outer edges, two near the PM center
- 1 mounted on the HOSS to simulate the BIA level

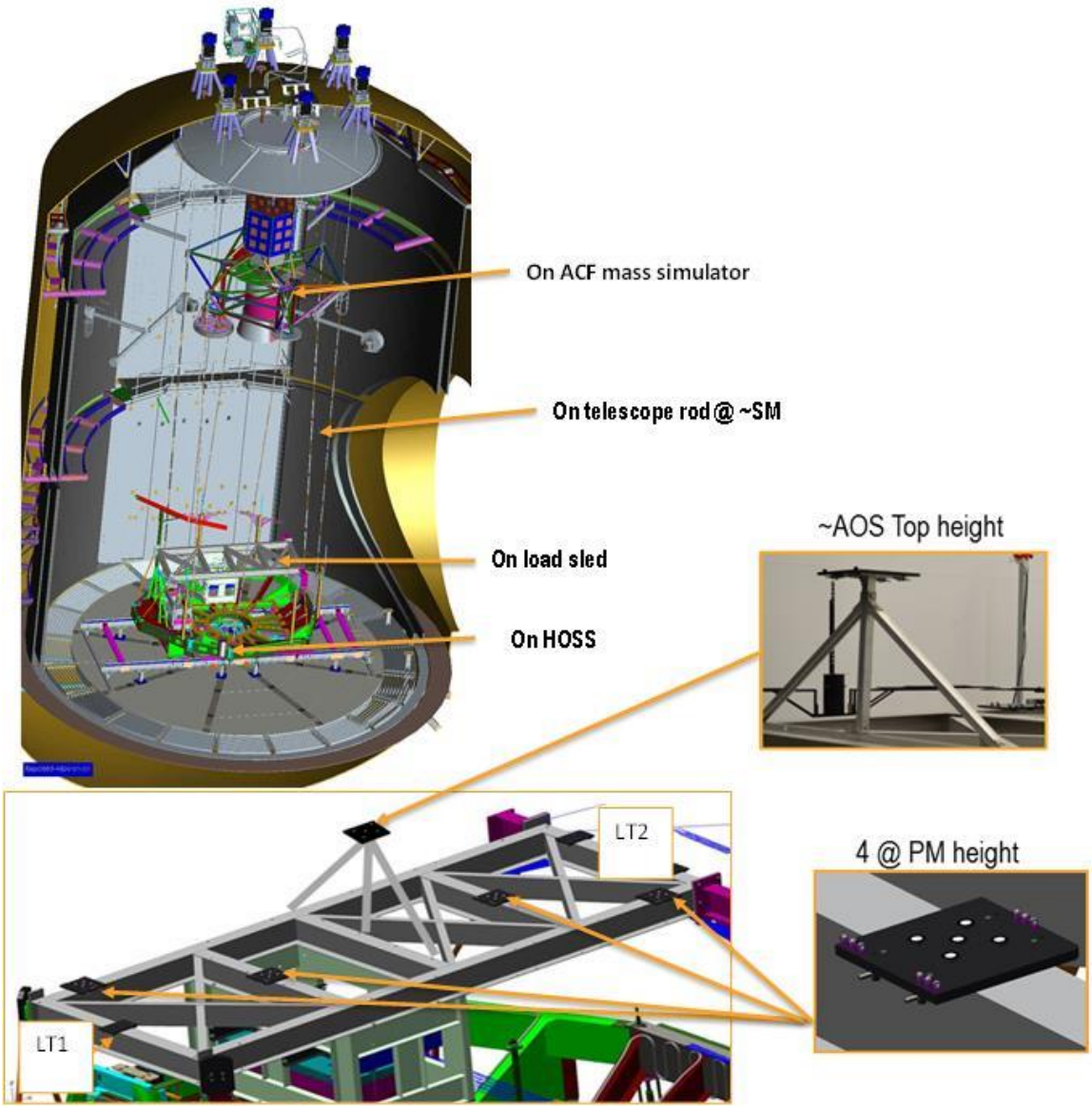

Figure 6. CAD drawing of PG calibration fixture arrangement with detail of load sled.

Two laser trackers were used during testing of the PG system to measure the absolute position of the calibration plates with respect to each other. The laser trackers are manufactured by Leica and two different models, AT-402 and 901 were used during the testing. They were attached to the load sled at positions LT1 and LT2 in Figure 6. PG calibration fixture arrangement with detail of load sled.

5.2 Pathfinder Optical Ground Support Equipment Test 1 (OGSE 1)

Measurements for CPM performance assessment were done on individual PG targets attached by mounting assemblies to various hardware points to support OGSE 1 testing. Unlike CCT, no additional calibration fixtures were used. Target assemblies vary in construction based upon the hardware to which it must interface. Figure 7 outlines the target assembly concepts and the hardware to which they interface.

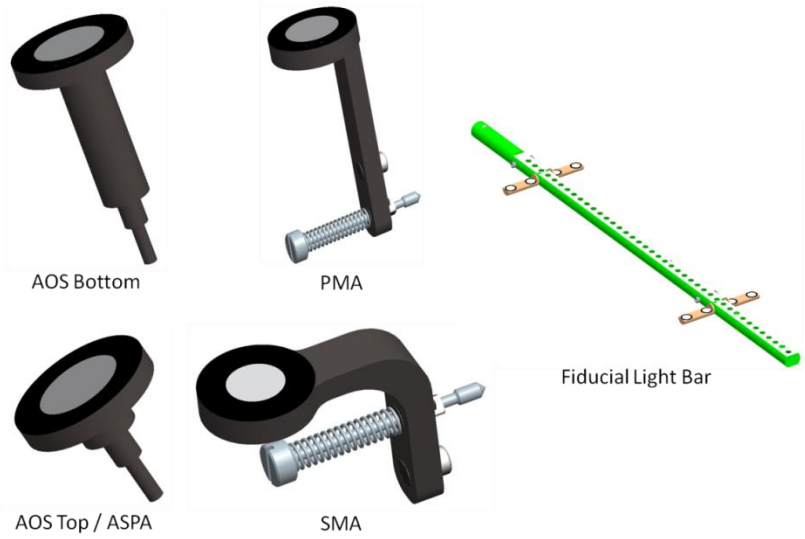

Figure 7. Target assembly examples

The specific targets measured were determined by both height in the chamber to match heights of interest (e.g. ASPA support arm targets are approximately the same height as the top of AOS once installed) and visibility to the laser radar (LR) system that was used as the reference for absolute accuarcy comapriosns. The following number of targets per hardware object were used in the analysis:

- Primary Mirror Segment Assembly PMSA – 7 of 9 targets
- Aft Optical Subsystem (AOS) flexure bushings – 3 of 3 targets
- AOS center hex – 5 of 6 targets
- AOS Source Plate Assembly (ASPA) support arm – 5 of 6 targets
- Secondary Mirror Assembly SMA – 4 of 5 targets (NOTE: LR could only measure back of PG mount)
- Piston sensors – 16 of 48 targets (one per sensor)
- Fiducial Light Bar FLB – 13 of 48 targets (3 each on 4 bars)
- Strut base – 5 of 6 targets
- Scale bars (vertical) 5 of 40 targets (1 pair on each of 2 bars + 1 additional bar)
- Scale bars (horizontal) 13 of 140 targets (1 pair on each of 5 bars + 3 additional bars)

5.3 Laser Radar

A Nikon Metrology Laser Radar system (MV-300) was used to directly measure the PG targets to provide an independent measurement of the PG target locations. The laser radar system was mounted on a Brunson stand on the rails on the +V3 side of the PMBSS. The laser radar scans the surface of the PG target as shown in Figure 8. Processing of the scanned PG target data is performed in the Spatial Analyzer software (SA) to produce a single value for the center of each measured PG target. The laser radar data acquisition and processing was performed by NASA GSFC (Jeff Gum, Joseph Hayden, Manal Khreishi, and Joss Lutter.) The laser radar was moved to two locations by raising the radar in the Brunson stand, thereby producing multiple measurements of the same target from different view angles.

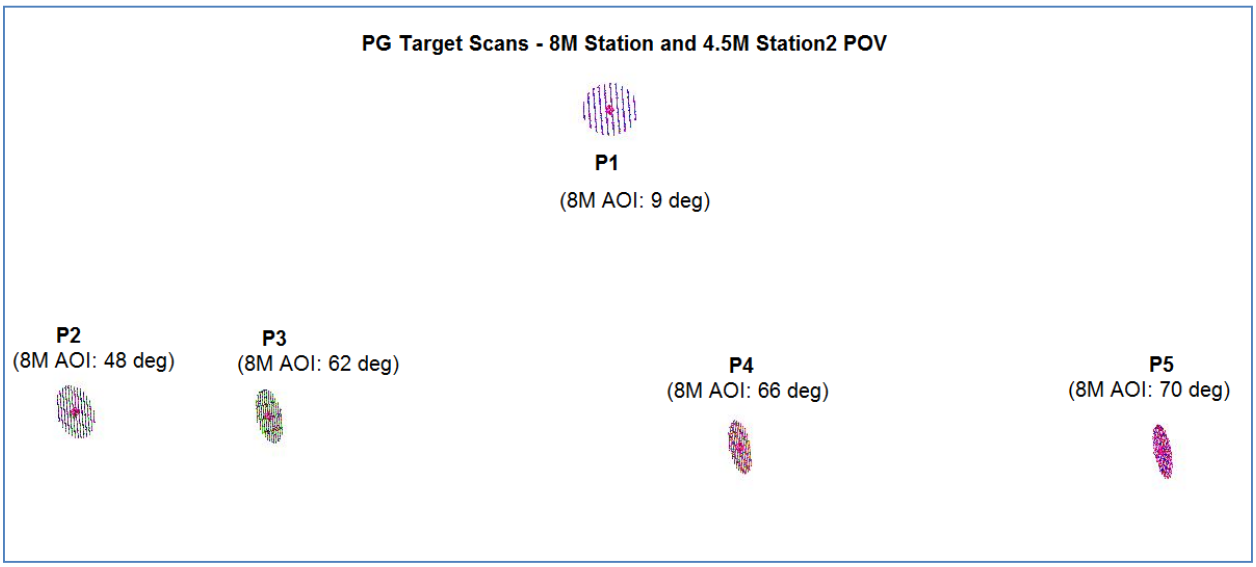

Figure 8. Illustration of radar measurements of PG targets

6. MODEL RESULTS AND APPLICATIONS

6.1 Hardware configuration, target placement, and data flow testing

Prior to the completion of the CPM, the modeled imagery was used to determine optimal camera pointing schemes to ensure that all objects were adequately sampled and to assess the expected accuracy of the system. Two camera pointing schemes were developed, - one that samples the whole chamber, and one that provides for more accurate determination of objects at or below the PM plane by not recording images of the ACF. Both of these pointing schemes were used successfully without modification during CCT and OGSE1 testing. A small modification was made to the lower chamber pointing scheme was made during OGSE2 to provide better imaging of the SM targets.

The DIRSIG model provided the ability to assess impact of changes made in the number of targets and the answer other configuration questions such as the true utility of having vertical scale bars on the telescope rod sleeves if the materials properties could be overcome. For instance, originally 120 targets were proposed for the PM, but that number was eventually reduced for the final OTIS design to 30. V-STARS analysis using simulated imagery of the two cases indicated that the same level of accuracy would be expected. In the case of the vertical scale bars, the model showed that they were poorly seen and would be expected to have a very large uncertainty and so would not provide reliable scale values.

The ability to exercise the analysis software to ensure that there were no issues with the number of images required and the spacing and placement of code targets, etc. proved quite useful prior to actual chamber testing as it allowed very quick turnaround of the initial data without having to work out logistics, fitting parameters, etc. at that time. The necessity of multiple code target sizes in the chamber to accommodate the large difference in distance, and hence reflectivity, between the closest and furthest sets required add capability being added to the V-STARS software to handle the combination of different sized targets during bundle adjustment. Using the modeled data, the new capability was tested out prior to actual chamber measurements. Having the model data available also allowed the determination of the pros and cons of various coordinate fitting schemes in terms of number of objects used and so the best accuracy could be assured.

6.2 Prediction of PG accuracy

There are several ways to estimate the expected accuracy of the CPM system based on the DIRSIG modeled imagery. Overall numbers can be calculated based on the image residuals or RMS of the bundle adjustment uncertainty. More detailed analysis of each object can be obtained by looking at point by point comparison of the V-STARS calculated bundle versus the reference values. Note: throughout this paper, uncertainties of point positions of targets in an object are reported as 1 sigma values, while bundle adjustment and measurement uncertainties are reported as 2 sigma values. This is because the latter is used for requirements comparison and requirements were specified in terms of 2 sigma.

6.2.1 Accuracy estimate based on image residuals

Another statistic reported by the V-STARS software is image residuals. The image residuals are a reflection of the variability in the value of the PG measurement of an individual target point in all the images that contain that point. Image residuals were ~0.73 µm for the DIRSIG modeled imagery, while GSI predicts their camera would be ~0.25 µm for the bundle adjustment. Image residuals are measured with respect to the dimensions of a pixel on the sensor, which is 10 µm (Table 1). For ISIM testing, measured in test residuals were 0.2527 µm.[7]

Another approach to estimating the expected measurement uncertainty is to extrapolate based on V-STARS image residual numbers. The DIRSIG model images showed significantly larger residual values than the corresponding ISIM imagery. The residual values were used as the magnitude of the uncertainty and then that magnitude was projected into object space at the distances indicated in the graph in

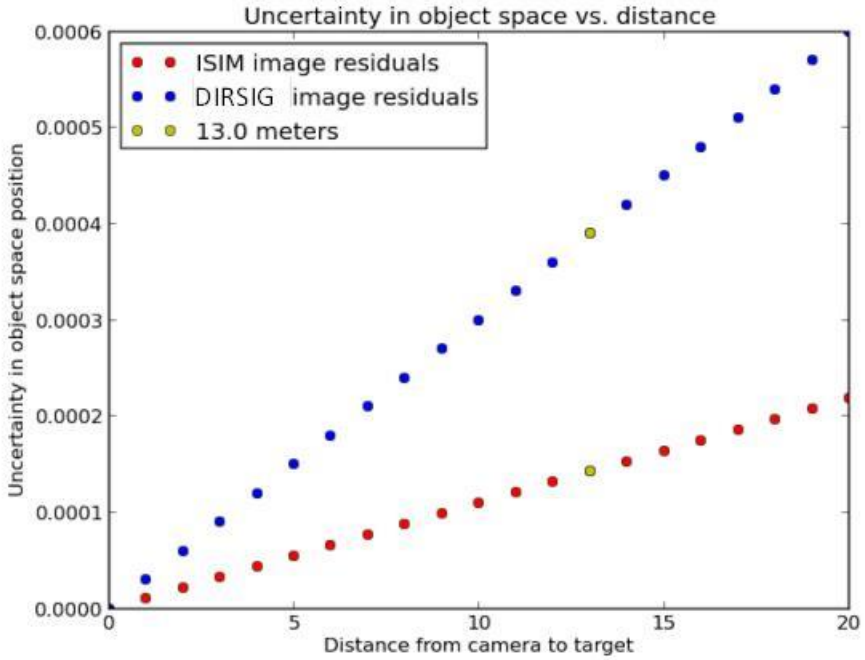

Figure 9 using the basic optics relationship of the height of an object on the image plane at a fixed focal length to the actual height of an object. In equation form

$$\sigma_o = \frac{\sigma_i * d}{f} \tag{4}$$

where σ_o is the uncertainty in object space, σ_i is the uncertainty in the image, d is the distance between the camera and the object, and *f* is the focal length.

The projected uncertainty from the modeled imagery is about 4 times that of the ISIM system or about 0.4 mm, 2 sigma. The projected uncertainty from the ISIM line is ~0.120 µm. These values are similar to that determined by using [6] (Section 6.2.2) and suggests that the overall image residuals of the actual system will be a main determinant of the actual accuracy of the CPM.

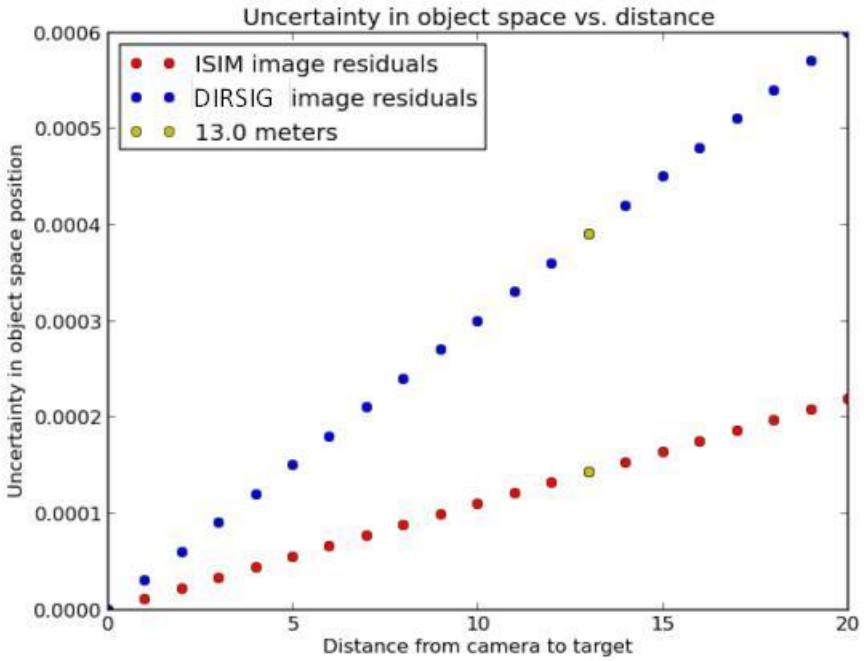

Figure 9. Projection of predicted measurement uncertainty calculated from image residual values reported by V-STARS as a function of target distances. Distance units are in meters and values are 2 sigma. The highlighted points correspond to 13 m, which is the distance from the top of the camera boom to the bottom of the AOS

6.2.2 Accuracy estimated based on bundle adjustment uncertainty

In order to be able to predict system performance accuracy, estimates were made using the DIRSIG processed results. One of the key numbers obtained from the modeled imagery was the bundle adjustment uncertainties as the overall PG error budget allowances were based on these. A table of the uncertainties obtained for various objects is given in the table below.

Table 2**.** Bundle adjustment uncertainties of simulated OTIS imagery. Values are 2 sigma

	2σ V1 (mm)	2σ V2 (mm)	2σ V3 (mm)	Magnitude (mm)
ACF	0.048	0.051	0.053	0.088
AOS (top)	0.054	0.032	0.031	0.070
PM	0.054	0.029	0.029	0.068
SM	0.043	0.035	0.037	0.067

The bundle adjust uncertainty can be used to determine a distance measurement uncertainty following the work of Blaha & Sandwith.[6] The 1 sigma distance uncertainty can be estimated by:

$$\sigma_d = \text{ppm} * L_{max} \quad (1)$$

Where ppm is the estimated uncertainty of the PG bundle adjustment in parts per million and $\boldsymbol{L_{max}}$ is the longest distance to be measured, and $\boldsymbol{\sigma_d}$ is the standard deviation of the measured PG value from an independent measure such as a laser tracker. If scaling error is small compared to point-point error, then point and distance uncertainties are equivalent. The volume to be measured in OTIS is quite large, as shown in Figure 10 below.

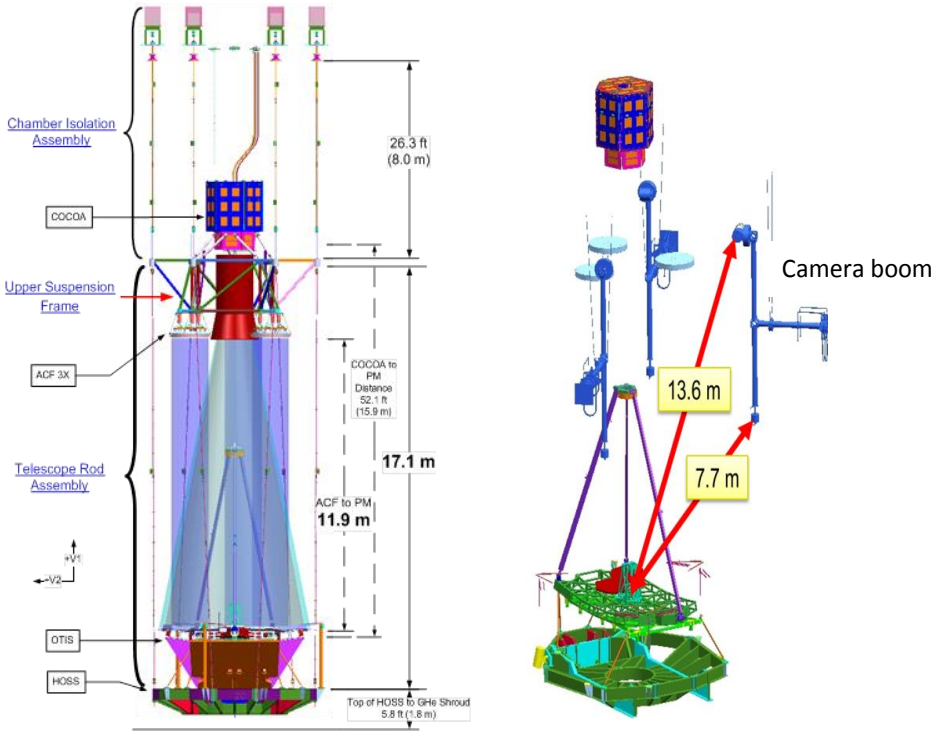

Figure 10. Dimensions of OTIS configuration

Using an approximation of 0.04 2 sigma or 0.02 mm1 sigma as the bundle adjustment uncertainty from Table 2, the predicted $\sigma_d = 20 * 13\text{m}=0.26$ mm 1 sigma or 520 mm 2 sigma.

For comparison, a previous test of the Integrated Science Instrument Module (ISIM) hardware utilized a similar photogrammetric setup to measure targets and the results are described in [7]. Part of the commissioning included laser tracker measurements of the PG targets. For ISIM testing, L_{max} was 3 m and the cross over results of the laser tracker versus PG measurements gave $\boldsymbol{\sigma_d}$= 0.012 mm for the measurement uncertainty. Using Eq. 1 to estimate the overall measurement error in parts per million (ppm):

$$\text{ppm error} = \frac{\sigma_d}{L_{max}} = \frac{0.012\text{mm}}{3000\text{ mm}} = 4\text{ ppm} \quad (2)$$

For OTIS, L_{max} = ~13 m so if we use the above ppm level as an estimate of the best case limit that can be expected for the PG measurement and back-calculating σ_d

$$\sigma_d = 4\text{ ppm} * 13\text{ m} = 0.052\text{ mm or 2 sigma} = 0.106\text{ mm} \quad (3)$$

The calculated value of the best case estimate compares very favorably with the GSI rating of the INCA3 cameras used in this system of 5 µm + 5µm/m which would give a prediction of 0.07 mm (1 sigma) or 0.14 mm (2 sigma) at 13 m as the measurement uncertainty. The modeled imagery and estimates based on the smaller scale ISIM tests provided a range of expected accuracy of the system.

6.2.3 Accuracy estimate based on point to point comparison

In order to determine if the OTIS PG bundle solution allowed for the desired level of uncertainty in absolute measures, comparison was made between the bundle adjustment values and driver file values to gauge the error and uncertainty at each point and the uncertainty in measuring distances between objects (e.g. AOS to SM). The driver file is the input file used to provide the CAD measurements of target locations for the DIRSIG model during V-STARS analysis.

Because there is an absence of absolute control coordinates in the adjustment, there will always be some small mismatch between the bundle adjustment axis and origin with real world physical values. In order to align the origins of the coordinate systems of the bundle and the desired V1, V2, V3 measurement axes, Monte Carlo Transformation Uncertainty (MCTU) based software[5] was used to align the two bundles using all objects to ensure the best possible fit. Once the transform was applied, the differences between all points in all objects was then determined, and the average difference and standard deviation calculated for object groups of points.

Table 3. Predicted error using modeled DIRSIG imagery of selected objects. Values are calculated for all PG targets that comprise an object.

	Avg ΔV1 (mm)	Avg ΔV2 (mm)	Avg ΔV3 (mm)	Magnitude	σV1 (mm)	σ V2 (mm)	σ V3 (mm)	Magnitude
ACF	-1.056	0.016	0.047	1.057	0.055	0.255	0.268	0.374
SM	0.187	-0.010	0.018	0.187	0.146	0.110	0.117	0.217
AOS	0.022	-0.006	-0.075	0.078	0.231	0.064	0.096	0.258
PM	0.129	-0.0004	-0.004	0.129	0.136	0.251	0.230	0.367

The overall magnitude of the distance uncertainty for the AOS and SM are similar to the 0.26 mm calculated based on the adjustment uncertainties in Section 6.2.2. That calculation assumed a symmetric distribution of error on each axis, which is clearly not the case, so the larger error for the PM may be due in part to the asymmetry. Scale is also a factor as discussed in 6.3. Due to the lower requirements of accuracy of ACF points than SM, AOS, and PM, there were much lower number of images devoted to the ACF versus objects lower in the chamber and so the higher ACF distance uncertainty is expected.

6.3 Scale effects

Another effect of the larger residuals and bundle adjustment uncertainties obtained with the model imagery was a sensitivity of the accuracy to the selection of scale bars. When the initial model comparison was made using all scale bars (invar and telescope rods) to define scale, large errors, on the order of a few millimeters, were observed on several of the objects as can be seen in Table 6. V-STARS applies a single scale factor to all data in the bundle, and examination of the bundle data showed that there were large uncertainties associated with many of the scale bar points for the bars on the telescope rods, presumably due to the fact that the targets are more oblique and therefore more prone to issues with accurate centroiding in some camera orientations. Removal of the telescope rod scale bars from the bundle scale estimate and use of only the horizontal invar bars resulted in a considerable improvement in accuracy, as seen in line two of

Table 5.

Table 4. Description of V-STARS run input for shortened designations used in Table 2

Designation	Subset of scale bars used to determine scale
All bars	All available scale bars (telescope rods and invar) included in the bundle to determine scale
all invar	Only the invar bars around the PM included in the bundle to determine scale
18 invar	Only the best 18 invar bars based on scale uncertainty < 0.05 mm
Best unc bar	Only a single scale bar which gave the lowest predicted uncertainty

Table 5. Predicted average error and standard deviation of PG measurement to actual position based on V-STARS bundle output of the PM points vs. driver file position. "_D" refers to the driver file reference. NOTE: Values are 1 sigma

Experiment	Groups: PM to PM_D		
	σ X (mm)	σ Y (mm)	σ Z (mm)
All bars	8.8365	8.8653	0.2130
all invar	0.4064	0.4343	0.1295
18 invar	0.3810	0.4089	0.1295
Best unc bar	0.2296	0.2512	0.1285

In order to confirm that at least some of the error was due to scale, Spatial Analyzer (SA) was used to fit the PG generated points in each object to the known values of each object and thus remove scale effects. The average error reduces to zero, and the standard deviations are a reflection of the residual uncertainty of the system. Comparison of different V-STAR runs to the "best uncertainty" bar data with scale removed is shown in Table 6. The scale removed data is highlighted in gray. In addition, the scale factors calculated by SA for each object are given. The calculated scale factors are not the same for each object, the largest difference is between the PM and SM and is 0.0285% or 285 PPM. Though this difference is small on an absolute scale, it is large with respect to the desired measurement tolerances which are on the order of 100 PPM and drove a criterion used during hardware testing of not using any scale bar whose measured error was more than 50 µm of the CMM value.

Table 6. Comparison of 1 sigma uncertainty for various configurations vs. residual uncertainty after scale is removed

Experiment	PM			SM			ACF		
	σX (mm)	σY (mm)	σZ (mm)	σX (mm)	σY (mm)	σZ (mm)	σX (mm)	σY (mm)	σZ (mm)
All invar	0.406	0.434	0.130	0.104	0.097	0.150	0.142	0.140	0.033
Best unc bar	0.229	0.252	0.129	0.102	0.099	0.155	0.271	0.259	0.036
Best unc bar Scale removed in SA	0.161	0.163	0.128	0.101	0.090	0.134	0.073	0.048	0.034
Scale Factor from SA	1.000083			0.999798			0.999854		

7. COMPARISON OF MODEL RESULTS TO OBSERVED PERFORMANCE

7.1 Image residuals

For the commissioning tests, the bundle adjustment of imagery from the CPM gave an overall image residual of 0.18 which is a similar magnitude to that found in [7] for the ISIM testing of 0.257 µm. The contribution to image residuals due to model limitations of, for instance, the target center visibility at oblique angles, is the most likely cause of the over-prediction. Because the image residuals are in line with both the manufacturer's expectations and the ISIM results, the

absolute accuracy of the CPM would be predicted to be at a level more consistent with the lower line in

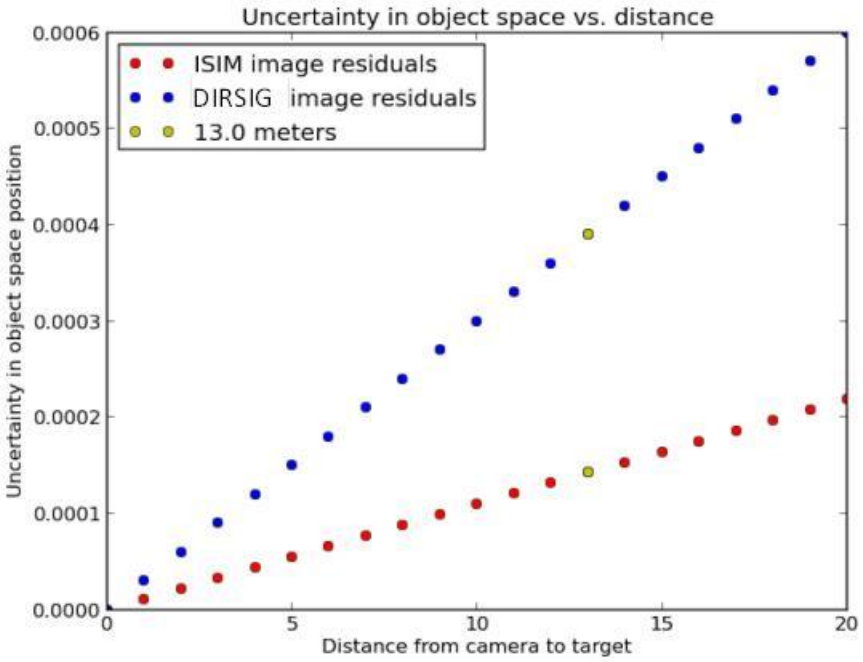

Figure 9, or a distance uncertainty of about 0.1 mm 2 sigma at the PM level.

7.2 Bundle adjustment uncertainty

During Chamber Commission Testing (CCT), 4 consecutive PG runs were obtained under both ambient and cryogenic conditions. The actual bundle adjustment uncertainties of a representative run are shown in Table 7

A few areas are similar (e.g. SM V2/V3), but in most cases the simulated imagery bundle adjustment uncertainties were a factor of 2-3X worse than measured in the chamber. It should be noted that bundle adjustment uncertainty does not necessarily translate to increased absolute error, as the bundle adjustment uncertainty is a measurement of variability image to image of the point measurements and a large distribution does not necessarily imply a shifted mean value. The mean value is the absolute position in space.

The actual vs. model predicted bundle adjustment uncertainties are quite consistent with the differences in the image residuals (section 7.1) of 0.75 to 0.18 mm with a similar level of decrease.

Table 7. Bundle adjustment uncertainties obtained from the first run of the PG commissioning testing. Model predictions are shown in parentheses.

	2σ V1 (mm)	2σ V2 (mm)	2σ V3 (mm)	Magnitude(mm)
ACF	0.012 (0.048)	0.011 (0.051)	0.011 (0.053)	0.020 (0.088)
SM	0.011 (0.043)	0.032 (0.035)	0.029 (0.037)	0.045 (0.067)
AOS (top)	0.016 (0.054)	0.009 (0.032)	0.009 (0.031)	0.020 (0.070)
PM	0.020 (0.054)	0.01 (0.029)	0.010 (0.029)	0.024 (0.068)

7.3 Point to point comparison

To provide an independent characterization of the absolute accuracy of the CPM system, laser trackers and laser radar systems were utilized at different times in the test program. The CPM testing consisted of 4 consecutive PG runs with

concurrent laser tracker or laser radar measurements. Prior to installation in the chamber, the laser radar measurements of many targets were also taken in the clean room. The run-to-run repeatability and absolute accuracy with respect to a laser tracker or laser radar based reference position were calculated for each run and also compared across runs.

Laser Tracker data was taken in the chamber. Laser Radar data was obtained both in the clean room and in the chamber. Due to the constraints of where the LR could be put in the chamber and the fall off with accuracy as a function of laser angle of incidence, some targets could only be measured in the clean room where the LR could be positioned more freely. Some pieces of hardware, e.g. FLAB were not installed in the cleanroom and so were only measured in the chamber. For the SM set of targets, even in the clean room the top could not be measured, and so the back of the PG target was measured and the PG center calculated based on design measurements of the target mount.

The measured vs. predicted values are shown in Table 8. The measured errors include both the PG and independent metrology uncertainties. The average error is consistent from the model to actual measurements within the uncertainty. The uncertainty decreases from the model to actual measured values to a level that is consistent on individual axes with the 3X change in image residuals, and is roughly 2X in overall magnitude. The individual axes uncertainty of the PM compares well to the 0.1 mm predicted in Section 6.2.1 and for the experimentally observed level of image residuals.

Table 8. Actual error from CCT measurements vs. predicted error using DIRSIG imagery (in parentheses) for selected objects. Values are 1 sigma. ACF numbers are from CCT data, SM, AOS, and PM from OGSE1 data. Data is from a single photogrammetry run.

	Avg ΔV1 (mm)	Avg ΔV2 (mm)	Avg ΔV3 (mm)	Magnitude
ACF	-0.575 (-1.056)	0.08 (0.016)	0.013 (0.047)	0.581 (1.057)
SM	0.086 (0.187)	--- (-0.01)	--- (0.018)	0.086 (0.187)
AOS	-0.075 (0.022)	0.054 (-0.006)	0.019 (-0.075)	0.094 (0.078)
PM	-0.045 (0.129)	-0.104 (-0.0004)	-0.023 (-0.0035)	0.116 (0.129)

	σ ΔV1 (mm)	σ ΔV2 (mm)	σ ΔV3 (mm)	Magnitude
ACF	0.15 (0.055)	0.52 (0.255)	0.475 (0.268)	0.72 (0.374)
SM	0.043 (0.146)	--- (0.11)	--- (0.117)	N/A (0.217)
AOS	0.045 (0.231)	0.101 (0.064)	0.151 (0.096)	0.187 (0.258)
PM	0.102 (0.136)	0.085 (0.251)	0.112 (0.23)	0.174 (0.367)

Another important measure of PG system performance is the repeatability of measurement. The 4 runs taken CCT were used to determine accuracy were also used to calculate an RMSE on a per point basis for each object under ambient

conditions. During OGSE2 testing, five consecutive runs were taken under cryogenic conditions with real hardware to verify the performance. The repeatability was calculated by.

$$RMSE = \sqrt{\frac{\sum 2\sigma_i^2}{N}} \quad (4)$$

Where *i* is the i^{th} PG target position on the calibration fixture, σ_i is the standard deviation calculated for a given number of PG runs for the ith position, and N is the number of points.

Table 9.Values by hardware object for Run to Run repeatability of PG measurements. 2σ is calculated as per equation (4)

	2σ V1 (mm)	2σ V2 (mm)	2σ V3 (mm)	Magnitude (mm)
ACF	0.039	0.062	0.123	0.143
SM	0.038	0.020	0.057	0.071
ASPA (AOS top)	0.022	0.006	0.007	0.024
AOS-Base	0.020	0.015	0.013	0.028
PM-A4	0.011	0.005	0.008	0.014
PM-C4	0.021	0.009	0.011	0.025
Strut Base (HOSS)	0.116	0.024	0.053	0.130

The results in Table 9 were used in the final error budget assessment instead of bundle adjustment uncertainties as these numbers better reflect the total measurement variability of the CPM. The full error budget includes not only uncertainty from the PG measuring and processing, but also contributions from factors such as mount uncertainty, scale uncertainty, thermal effects, etc. The most stringent requirements for the OTIS T/V testing were ± 0.10 mm in piston and decenter at the PM level and ± 0.15 mm at the SM level. The full error budget prediction was 0.038 mm and 0.084 mm for PM piston and decenter, and 0.086 for SM piston, all well within requirements.

Also consistent with the change in image residuals, the scale bar uncertainty and errors decreased dramatically as shown in Figure 11. The modeled scale bar data resembles the actual vertical scale bars in both uncertainty and trend in errors, though there is also a cluster of scale bars with a noticeable bias in the model data. Since only scale bars with less than 0.05 mm in error are used to determine scale of the bundle, the cluster of anomalous bars would not affect the resulting measurement values of objects in the chamber.

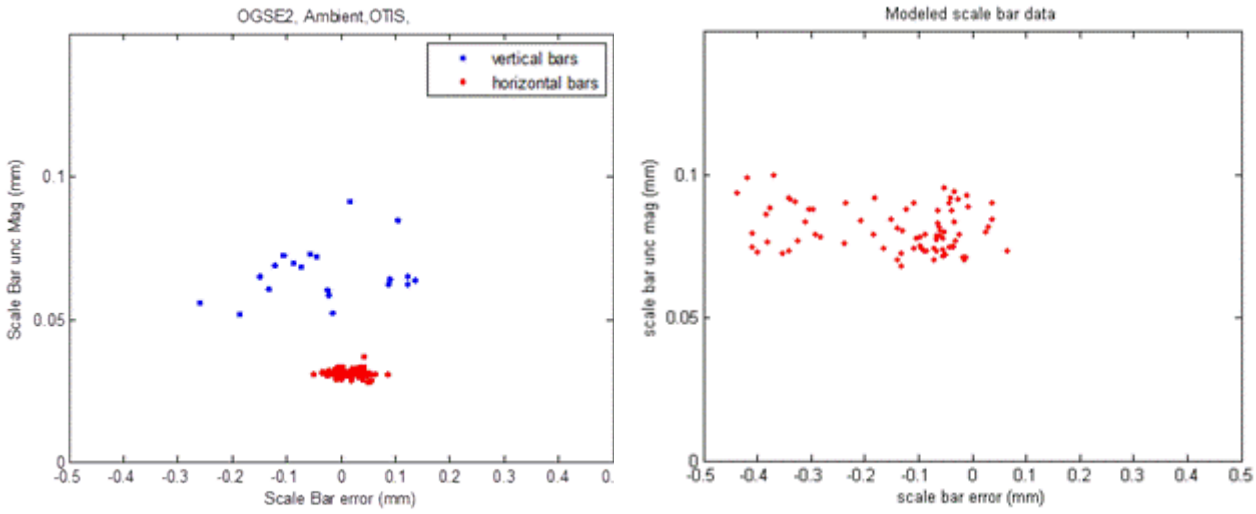

Figure 11. Comparison of bundle uncertainty magnitude (RSS of 1 sigma x, y, z values) and scale bar length error (PG measured scale bar length vs. actual length)

The lack of availability of known reference points under cryogenic conditions besides the scale bars prevented extensive characterization of the absolute accuracy under those conditions. However, the Strut Base Points Targets (SBT) on the HOSS do provide such a reference. SA was used to fit SBT for ambient and cryogenic runs from OGSE1 and OGSE2. For the SBT points a repeatability of 50 μ m was achieved for an object of 7 m diameter. The observed shrinkage of the HOSS was 2.8 parts per thousand or 0.28% as determined by the difference in scale factor needed to match the shrinkage from ambient to cryogenic conditions. The expected shrinkage was 0.3%. The difference in scale factor predicted from OGSE1 to OGSE2 was 7 ppm which is an overall difference of 0.05 mm between the two tests and consistent with the repeatability in the V2/V3 axes given in Table 9.

8. CONCLUSIONS

The close range photogrammetry system that is used in T/V testing of JWST hardware was modelled extensively prior to construction in order to verify performance, define camera pointing schemes, and assess effects of various proposed target configuration. This was accomplished years before the actual test will be completed. A computer generated DIRSIG model predicted a higher level of image residuals and measurement uncertainty then observed in the actual system, but correctly predicted the error in absolute measurement. When the difference between model and actual image residuals are accounted for, the measurement uncertainty from the DIRSIG model is similar to that found in chamber T/V verification testing. Further DIRSIG model simulations can be improved by better camera characterization in order to better simulate down-sampling and noise from the cameras.

The CPM system was predicted by the DIRSIG model to meet the requirements of the error budget and in-chamber testing confirmed those predictions. The measurement uncertainty of the CPM is < 0.1 mm, the absolute positional accuracy at the AOS and PM level is <0.1mm, and the absolute positional accuracy is <0.15mm at the SM level. The CPM has been successfully used in 3 chamber tests and will be used in the final OTIS testing phase.

9. ACKNOWLEDGEMENTS

The optical test design, preparation, and execution was supported by the JWST contract NNG11FD64C with NASA GSFC. The JWST system is a collaborative effort involving NASA, ESA, CSA, the Astronomy community and numerous principal investigators.

REFERENCES

[1] Hill, M. D., Herrera, A. A., Crane, J. A., Packard, E. A., Aviado, C. G., & Sample, H. P., "Alignment measurements of the Microwave Anisotropy Probe (MAP) instrument in a thermal/vacuum chamber using photogrammetry," Proc. SPIE 4131, 255-265 (2000).

[2] Nowak, M., Cleveland, P., Crane, A., Davila, P., Herrera, A., Hylan, J., Liehr, A., March J., Ohl, R., Redman, K., Sampler, H., Stock, J. Wenzel, G., Woodruff, R., Young, P., "Verification of the James Webb Space Telescope Integrated Science Instrument Module Cryogenic Structural Alignment Requirements via Photogrammetry," Proc. of SPIE, 7068, (2008).

[3] Whitman, T. L., Wells, C., Hadaway, J. B., Knight, J. S., Lunt, S., " Alignment test results of the JWST Pathfinder Telescope mirrors in the cryogenic environment," Proc. of SPIE, 9904, (2016).

[4] *DIRSIG*. (n.d.). Retrieved from DIRSIG Website: http://www.dirsig.org/

[5] Hayden, J., Kreishi M., Hadjimichael, T., Ohl, R., "Monte Carlo Method for Uncertainty Propagation in JWST Metrology Databases." Quality Digest Proc. CMSC, http://www.qualitydigest.com/inside/cmsc-article/052115-monte-carlo-method-uncertainty-propagation-jwst-metrology-databases.html (5 May 2016)

[6] Blaha, G., and Sandwith, S. C., "Methodology for accuracy assesments and verifications in digial photogrammetry," Proc. SPIE 4189 , 218-228 (2001).

[7] Nowak, M. D., Cleveland, P. E., Cofie, E., Crane, J. A., Davila, P. S., Eegholm, B. H., Hammond, R. P., Heaney, J. B., Hylan, J. E., Johnston, J. D., Ohl, R. G., Orndorff, J. D., Osgood, D. L. Redman, K. W., Sampler, H. P., Smee, S. A., Stock, J. M., Threat, F. T., Woodruff, R. A., Young P. J., "Cryogenic perfomance of a high precision photogrammetry system for verificationof the James Webb Space Telescope Integrated Science Instrument Module and associated ground support equipment structural alignment requirements," Proc. of SPIE 7793, (2010).